PERGAMON

Continental Shelf Research 19 (1999) 845–869

CONTINENTAL SHELF RESEARCH

Numerical simulation of principal tidal constituents in the South China Sea, Gulf of Tonkin and Gulf of Thailand

Guohong Fang[a,*], Yue-Kuen Kwok[b], Kejun Yu[a], Yaohua Zhu[a]

[a]*Institute of Oceanology, Chinese Academy of Sciences, 7 Nanhai Road, Qingdao, 266071, People's Republic of China*

[b]*Department of Mathematics, Hong Kong University of Science and Technology, Clear Water Bay, Kowloon, Hong Kong*

Received 5 June 1998; accepted 19 August 1998

Abstract

The principal tidal constituents M_2, S_2, K_1 and O_1 in the South China Sea, Gulf of Tonkin and Gulf of Thailand are simulated simultaneously using the numerical scheme of Kwok et al. (1995 Proceedings of the 1st Asian Computational Fluid Dynamics Conference, pp. 16–19). The average differences between the computed and observed harmonic constants are mostly within 5 cm and 10° for amplitudes and phase-lags, respectively. The simulated tidal regimes in the present model are believed to be more accurate than the previous numerical results. Our studies confirm that a clockwise rotating M_2 amphidromic system lies in the southeast of the Gulf of Thailand and an S_2 amphidromic system at the near-shore area of the northeast South China Sea. The linear tidal energy equation developed by Garrett (1975 Deep-Sea Research 22, 23–35) is generalized to the nonlinear case. Based on the numerical results, the energy budgets in the South China Sea and its subareas, namely the Taiwan Strait, the Gulf of Tonkin, the Gulf of Thailand and the remaining area are investigated. The tidal motion in the Taiwan Strait is maintained mainly by the energy fluxes from the East China Sea for both semidiurnal and diurnal species and partially from the Luzon Strait for semidiurnal species. For the other parts of the South China Sea, the tidal motion is mainly maintained by the energy fluxes through the Luzon Strait. The energy inputs from the tide-generating force are negative for semidiurnal species and positive for diurnal species.

Keywords: Tides; Tidal energy; South China Sea; Gulf of Tonkin; Gulf of Thailand

*Corresponding author. E-mail: ghfang@ms.qdio.ac.cn.

0278–4343/99/$ – See front matter
PII: S0278–4343(99)00002–3

1. Introduction

The South China Sea is one of the broad marginal seas surrounded by the southeast Asian mainland and the Islands of Taiwan, the Philippines, Kalimantan and Sumatra (Fig. 1). The region consists of three main parts: the deep basin, the mainland shelf and the Sunda Shelf. The deep basin, covering about 1.5 million km^2, occupies the central-east part of the South China Sea with the greatest depth exceeding 5000 m. It has an opening, the Luzon Strait, on its northeast quadrant connecting it to the Pacific Ocean. Coral reefs are abundant in its south (Nansha Islands) and northwest (Xisha and Zhongsha Islands). The shelf region occupies about 55% of the South China Sea and can be divided into the mainland shelf in the north and the Sunda Shelf to the southwest. The mainland shelf lies to the northwest of the deep basin. The shelf extends about 200 km offshore and includes the Taiwan Strait to the northeast, which connects to the East China Sea, and the Gulf of Tonkin in the west. The Sunda Shelf has a width of about 700 km from the Malay Peninsula to its eastern edge. The Gulf of Thailand occupies its northwest part and the Karimata Strait links the South China Sea to the Java Sea.

In the deep basin the tidal patterns are very simple, and the tidal currents are very weak. In contrast, the tidal regimes on the shelf, especially the semidiurnal tides,

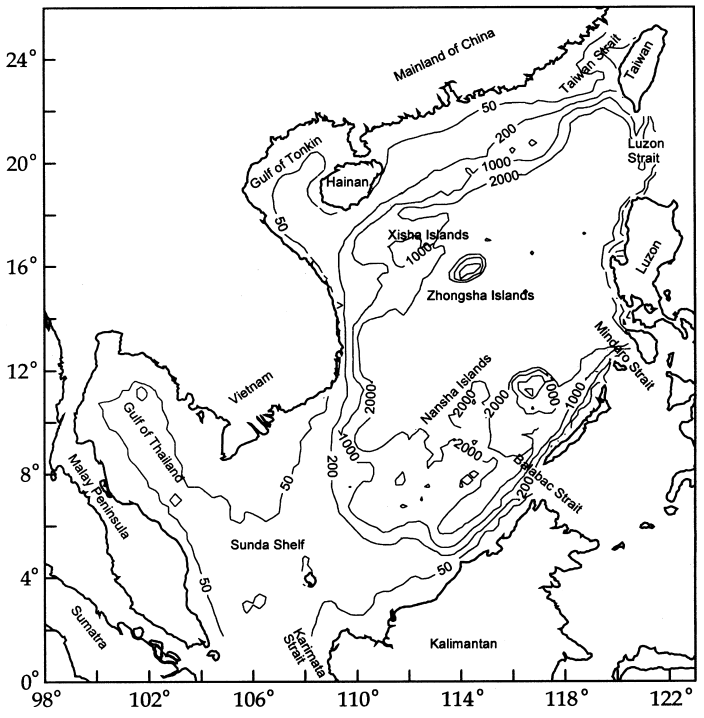

Fig. 1. Map of the South China Sea. The bottom depth is given in meters.

are complex and the tidal currents may be strong. The tides in the South China Sea, Gulf of Tonkin and Gulf of Thailand have been studied by numerous oceanographers (Dietrich, 1944; Bogdanov, 1963; Sergeev, 1964; Nguyen, 1969; Sager, 1975; Ye and Robinson, 1983; Yu, 1984; Fang, 1986). The cotidal charts drawn by different researchers before the 1980s revealed great diversity in shelf areas. The discrepancies among the published cotidal charts have been significantly reduced since 1980s. However, noticeable differences can still be observed.

The work by Ye and Robinson (1983) was the first successful numerical study on the tides in this area. The basic patterns produced from their model agree well with the observed ones. However, the observed phase-lags used for validating their model contained certain errors (generally 10–20° and up to 35°); and an incorrect phase for K_1 tide-generating potential was used. The latter leads to incorrect energy budget calculation. Furthermore, only M_2 and K_1 were studied and these constituents were simulated separately.

In the present paper we extend the study to include the S_2 and O_1 tides and simulate the constituents M_2, S_2, K_1, and O_1 simultaneously. Though the nonlinear terms are included in the numerical computation, we will only present the results of these four principal constituents in the present paper. Because the constituents M_2, K_1 and O_1 are nearly equally important in generating shallow water tides in the shelf areas of the South China Sea, the problem here is much more complicated than in the other shelf seas, such as in the northwest European shelf seas. A devoted effort will be made in the future to simulate and analyze the shallow water tides.

2. Numerical model

2.1. Governing equations

The governing equations used in the present study are the vertically integrated equations of continuity and momentum:

$$\partial_t \zeta = -a^{-1}[\partial_\lambda (Hu) + \partial_\phi (Hv\cos\phi)], \tag{1}$$

$$\partial_t u = -a^{-1}u\partial_\lambda u - R^{-1}v\partial_\phi u + R^{-1}uv\tan\phi + fv - rH^{-1}(u^2+v^2)^{1/2}u - ga^{-1}\partial_\lambda(\zeta-\bar{\zeta}) + A\,\Delta u, \tag{2}$$

$$\partial_t v = -a^{-1}u\partial_\lambda v - R^{-1}v\partial_\phi v - R^{-1}u^2\tan\phi - fu - rH^{-1}(u^2+v^2)^{1/2}v - gR^{-1}\partial_\phi(\zeta-\bar{\zeta}) + A\,\Delta v, \tag{3}$$

where t is time, λ and ϕ are the east longitude and north latitude respectively, ζ is the sea surface elevation above the undisturbed sea level, u and v are the east and north components of fluid velocity respectively, $\bar{\zeta}$ is the adjusted height of equilibrium tides, R is the radius of the earth, $a = R\cos\phi$, $f = 2\Omega\sin\phi$ with Ω representing the angular speed of earth's rotation, g is the acceleration due to gravity, $H = h + \zeta$ is the total

water depth with h denoting the undisturbed water depth, r is the bottom friction coefficient, A is the coefficient of horizontal eddy viscosity. In the above equations we use $\partial_t u$ to represent $\partial u/\partial t$ and use Δu to denote $a^{-1}[a^{-1}\partial_\lambda(\partial_\lambda u) + R^{-1}\partial_\phi(\cos\phi\partial_\phi u)]$. After a few trial simulations, the frictional parameters r and A are finally taken to be 0.002 and 1000 m^2/s, respectively.

2.2. Numerical scheme and computational grid

In the numerical computation, the governing Eqs. (1)–(3) are approximated by a set of finite difference equations proposed by Kwok et al. (1995). The numerical schemes are second-order accurate and can be solved with a time step significantly longer than that determined by the Courant–Freidrichs–Lewy condition, due to the application of the alternating direction implicit technique. An outline of the scheme is given in the Appendix.

The computational mesh is shown in Fig. 2. The grid size is $0.25^\circ \times 0.25^\circ$ and the coverage of the computational area is larger than that of Ye and Robinson (1983). The

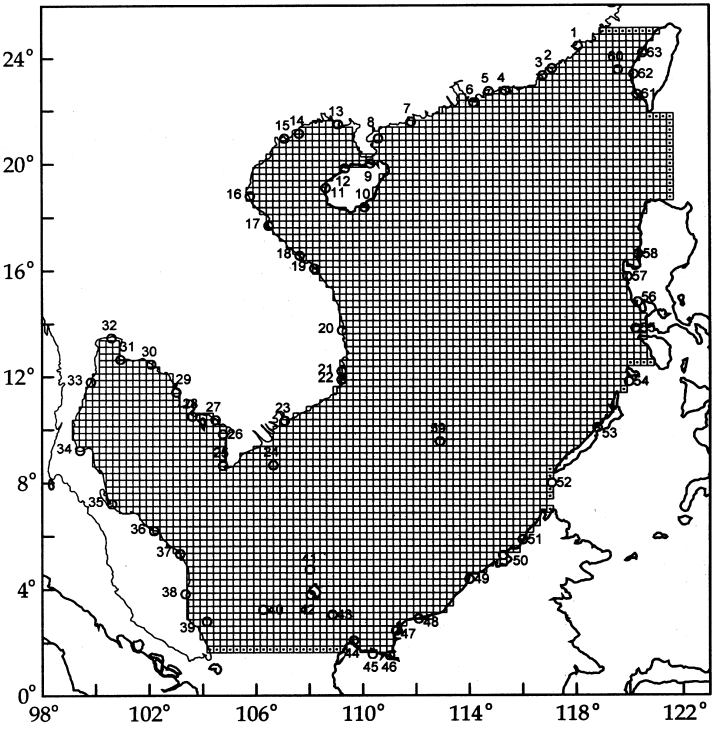

Fig. 2. Computational grid. The dots indicate the ζ-points on the open boundaries where the tidal elevations are given as functions of time. The open circles indicate the land-based tidal stations where the tidal harmonic constants are available and to be used for model verification. The names of these stations are listed in Table 1.

computational domain has three large openings located at the northern Taiwan Strait, Luzon Strait and northern Karimata Strait. A few other small openings lie at/near the Mindoro Strait and Balabac Strait. Here we extend the computational area to include most part of the Taiwan Strait, because the semidiurnal tides have important structures in the southwest of the Strait. We will see later that an M_2 nodal band and an S_2 amphidromic system are present in the southern entrance of the strait.

2.3. Boundary conditions and equilibrium tides

In the present study the Beijing standard time (referred to the meridian of 120°E) will be adopted throughout. The four principal constituents are simulated simultaneously. Along the open boundaries, the heights of the water surface are given at the ζ-points as

$$\zeta = \sum f_C H_C \cos[\omega_C t + (V_0 + u)_C - g_C] \tag{4}$$

where H and g are harmonic constants for the amplitude and phase-lag respectively, the subscript C stands for either one of the constituents: M_2, S_2, K_1 or O_1; ω is the angular speed of the tidal constituents, f the nodal factor, u the nodal angle, V_0 the initial phase angle of the equilibrium tide.

The harmonic constants on the open boundaries at the Balabac Strait and Mindoro Strait are calculated simply through linear interpolation from the values at the nearby tidal stations. Those on the open boundaries across the Taiwan Strait and Karimata Strait are taken from existing model results (Fang et al., 1984) and empirical charts (Cao et al., 1997). The open boundary values at the Luzon Strait play the most important role in accurately reproducing the tidal distribution in the South China Sea. The harmonic constants at totally 5 tidal stations (3 on the southern coast of Taiwan and 2 on small islands to the southeast of Taiwan) are used to determine the values at the northern end of the boundary, and the harmonic constants at 3 tidal stations on the northern coast of the Luzon Island are used to determine the values at the southern end. The harmonic constants at Basco (20°27′N, 121°58′E), which is located at the Batan Island, nearly the mid-point of the Luzon Strait, enable us to make parabolic interpolation for the boundary condition. The harmonic constants at the above-mentioned tidal stations are taken from the Admiralty Tidal Tables.

Along the closed boundaries, the normal component of the flow vanishes. Along the entire boundaries, a free-slip condition is specified by assuming $A\partial u_s/\partial n = 0$, where s and n denote the tangential and normal directions to the boundary respectively.

The heights $\bar{\zeta}$ in Eqs. (2) and (3) are the equilibrium tides multiplied by the factor 1-k-h, where k and h are Love numbers due to the earth's elastic response and the redistribution of the earth's mass (Pugh, 1987). Corresponding to Eq. (4), $\bar{\zeta}$ is written in the form

$$\bar{\zeta} = \sum f_C \bar{H}_C \cos[\omega_C t + (V_0 + u)_C + (p\lambda + \omega_C S)], \tag{5}$$

where $S = -8$ h is the number of the Beijing standard time zone; $p = 1$ or 2 for diurnal or semidiurnal tide, respectively. According to Wahr (1981), the amplitudes $\bar{H}_C$ for various constituents are chosen as follows (in m):

$$\bar{H}_{M_2} = 0.168\cos^2\phi,\ \bar{H}_{S_2} = 0.078\cos^2\phi,\ \bar{H}_{K_1} = 0.104\sin 2\phi,$$

$$\bar{H}_{O_1} = 0.070\sin 2\phi. \tag{6}$$

The atmospheric tides have a distinguished semidiurnal solar oscillation. Its amplitude is about 10% of the astronomical solar tide. To take the effect of atmospheric tides into consideration, we add an additional term to the equilibrium tide for the S_2 constituent, this term is written in a form analogous to the astronomical tide as

$$\bar{\zeta}'_{S_2} = \bar{H}'_{S_2}\cos[\omega_{S_2}t + V_{0S_2} + (2\lambda + \omega_{S_2}S) - \alpha], \tag{7}$$

in which $\bar{H}'$ and α are equal to 0.0113 m and 112° respectively, according to Haurwitz (1956) (see Chapman and Lindzen, 1970, p. 34).

3. Model verification

The simulation begins from a state of rest ($\zeta = u = v = 0$) using time step Δt of 5 min. The simulation is carried out for 375 d, and the initial part of the computed time series of 10 d are discarded. Before the present multiple constituent simulation is carried out we made several single constituent runs. These showed that the fluid motion reached periodic oscillation after a simulation time of 10 d (10 periods for diurnal constituents, 20 periods for semidiurnal constituents). The criterion was that, the computed values of ζ, u and v differed from the corresponding values one period before by less than 0.001 m, 0.001 m/s and 0.001 m/s, respectively. The computed year-long time series of ζ, u and v are analyzed by a conventional tidal harmonic analysis program (Wang and Fang, 1981) to yield harmonic constants.

Along the coasts and on islands, we select 63 tidal stations for model verification. The position of these stations have been indicated in Fig. 2. Along the coasts of the China mainland, Hainan Island and Yongshujiao, the harmonic constants are taken from the archives of the Institute of Oceanology, Chinese Academy of Sciences. They are generally based on at least one-year observation and thus are sufficiently accurate. For the other areas, the harmonic constants are quoted from the British Admiralty Tide and Tidal Stream Tables. The quality of these data varies significantly. Especially in the Gulf of Thailand, the tidal stations are too sparse relative to the complicated structure of the semidiurnal tides. The harmonic constants at some stations (Kamau, Tammassu, Chandaburi, Satahib Bay and Songkhla) are obtained from the analysis using the Admiralty Method. This implies that the observation period are only 1 or 2 d.

The computed and observed harmonic constants are listed together in Table 1 for comparison. The average differences are generally small as shown in Table 2. The greatest discrepancy is the phase-lag of S_2. This can be partially attributed to the errors existing in the observed phase-lags due to small amplitudes.

4. Results and discussion

4.1. Distribution of the principal tidal constituents

The cotidal charts produced by the present simulation model for M_2, S_2, K_1 and O_1 are given in Figs. 3–6.

The M_2 chart (Fig. 3) obtained from the present study is very close to that of Fang (1986), which was drawn empirically based on the observed harmonic constants on coasts and islands. The basic pattern of the present result is also consistent with Ye and Robinson (1983). But generally our computed phase-lags are later than those of Ye and Robinson (1983) by about 15°, with distinguished differences in the Gulf of Thailand. The southern amphidromic point of Ye and Robinson is located near the entrance of the Gulf, and the phase-lags on the west coast of Vietnam are between 60 and 90°. The corresponding amphidromic point of the present study is located in the Gulf and the phase-lags on the west coast of Vietnam is between 120 and 150°. The observed phase-lags at Station Nos. 25–27 listed in Table 1 are closer to the results of the present study. The northern amphidromic point from the present computation is located at a latitude of about 11°20′N, while the corresponding point of Ye and Robinson (1983) appears to be degenerate (on land) and is located at about 9°20′N. The observed harmonic constants at Ko Raet and Koh Prap (see Table 1) clearly agree better with the present computation.

The M_2 tidal wave is a progressive wave in the deep basin, propagating southwestward from the Luzon Strait. The wave speed is approximately 120–170 m/s. This is an appropriate range for a long wave propagating in a channel with depths of 2000–3000 m. After the wave passes across the Sunda Shelf edge (Fig. 1) the wave speed is greatly reduced, and gradually the reflected wave becomes important. A nodal band can be observed along a line roughly corresponding to the axis of the Gulf of Thailand and extending to the west tip of Kalimantan (Borneo). This band is approximately 300–400 km away from the southern Malay Peninsula. A pair of amphidromic points appear in the northwestern part of this nodal band. The northern amphidromic point lies very close to the northern Malay Peninsula, and the amphidromic system rotates anticlockwise. The southern amphidromic system rotates in clockwise direction. It is very rare in the Northern Hemisphere. The right turning of the incident wave and low latitudes can be considered as the main causes.

The M_2 tide in the Taiwan Strait is generated jointly by incident Kelvin waves from the East China Sea and the South China Sea, with the former stronger than the latter. The wave from the East China Sea propagates southwestward and has higher amplitudes on the mainland side, resulting large tidal range in the northwestern

Table 1
Comparison between computed and observed harmonic constants for four principal constituents

				M_2				S_2				K_1				O_1			
				comp.		obs.		comp.		obs.		comp.		obs.		comp.		obs.	
No.	Place	N	E	H	g	H	g	H	g	H	g	H	g	H	g	H	g	H	g
1	Xiamen	24°27′	118°04′	77	348	184	352	53	44	54	44	34	284	34	281	28	237	27	238
2	Shaoanwan	23°36′	117°06′	57	13	76	14	17	92	18	80	28	291	34	292	24	240	30	248
3	Shantou	23°20′	116°45′	34	10	41	22	10	102	10	91	27	289	29	297	23	240	24	249
4	Shanwei	22°45′	115°21′	30	249	28	255	11	271	11	278	31	287	33	298	27	238	26	250
5	Dayawan	22°44′	114°44′	31	251	37	252	11	277	15	279	32	288	34	295	27	239	27	249
6	Hong Kong	22°18′	114°10′	38	256	38	265	14	287	15	294	33	290	36	297	28	240	29	249
7	Hailingshan	21°35′	111°49′	60	292	68	294	25	332	28	333	41	312	42	314	36	261	36	265
8	Naozhou I.	20°57′	110°35′	64	303	78	312	28	343	35	355	43	320	44	325	38	268	38	276
9	Haikou	20°01′	110°17′	27	265	20	264	11	329	12	328	34	80	39	96	44	14	49	34
10	Lingshuijiao	18°23′	110°04′	19	299	18	310	7	344	8	340	32	306	30	317	28	255	23	257
11	Basuo	19°06′	108°37′	15	56	18	61	5	118	6	118	49	59	54	71	60	356	62	11
12	Yangpu	19°50′	109°20′	18	139	24	150	6	208	9	204	69	76	73	85	81	10	81	18
13	Beihai	21°29′	109°05′	35	177	44	177	10	250	11	237	85	85	88	96	95	19	96	34
14	Tsieng mum	21°08′	107°37′	22	177	18	179	5	238	6	230	79	89	73	96	90	22	82	30
15	Hongai	20°57′	107°04′	6	125	6	144	4	143	3	147	69	92	85	103	80	25	88	48
16	Hon Nieu	18°48′	105°46′	25	39	30	31	11	118	9	113	48	99	49	103	59	31	58	57
17	Quang Khe	17°42′	106°28′	19	22	18	41	6	97	5	91	26	96	21	110	37	28	27	53
18	Thuan An	16°34′	107°38′	17	339	18	351	5	21	4	58	9	315	3	270	8	1	2	19
19	Da Nang	16°05′	108°11′	18	320	17	330	7	1	6	10	22	301	20	304	16	257	13	258
20	Qui Nhon	13°45′	109°13′	16	315	18	321	7	357	6	7	32	306	34	315	27	254	27	268
21	Nha Trang	12°12′	109°12′	17	320	18	321	7	2	6	351	32	306	34	307	28	254	30	258
22	Cam Ranh	11°53′	109°12′	17	322	18	329	8	2	9	15	33	306	34	307	28	254	30	265
23	Vung Tau	10°20′	107°04′	74	47	79	63	22	94	30	111	57	323	61	327	42	268	46	277
24	Con Dao	8°40′	106°38′	77	78	79	81	23	142	27	142	65	345	64	333	42	288	46	288
25	Kamau River[b]	8°39′	104°45′	10	122	15	97	1	18	6	50	22	68	37	5	11	34	21	329
26	Tammassu[b]	9°50′	104°45′	26	136	11	135	2	47	6	00	33	65	28	40	15	25	15	14
27	Hatien	10°22′	104°28′	24	138	10	119	5	60	2	353	31	83	26	81	15	45	13	52
28	Ream	10°30′	103°36′	6	68	7	29	4	51	7	78	18	129	22	135	12	88	14	92
29	Kaoh Kong I.	11°25′	103°00′	11	85	12	51	6	94	6	123	38	159	37	161	22	109	27	131
30	Chandaburi[b]	12°28′	102°04′	16	141	15	125	8	179	6	312	61	178	58	174	33	125	46	129

31	Satahib bay[b]	12°39′	100°55′	26	181	24	159	15	234	9	267	70	186	64	176	37	133	46	129
32	Bangkok bar	13°28′	100°35′	49	200	55	170	29	249	27	242	81	191	67	182	41	137	46	131
33	Ko Raet	11°48′	99°49′	8	193	6	168	4	229	00	242	62	189	52	184	33	136	34	132
34	Koh Prap	9°13′	99°25′	20	0	18	358	9	59	12	86	52	199	46	197	29	145	30	144
35	Songkhla[b]	7°13′	100°36′	35	333	23	321	11	1	3	65	8	318	6	285	2	201	4	212
36	Tumpat	6°12′	102°10′	26	262	18	261	11	279	8	293	43	10	28	351	19	324	17	316
37	Trengganu	5°21′	103°08′	38	243	27	243	12	266	12	289	61	12	52	3	30	326	30	315
38	Kuantan	3°50′	103°20′	64	255	55	270	13	325	18	322	69	19	52	18	38	339	34	334
39	Pulau Tioman	2°48′	104°08′	50	264	58	274	14	345	18	327	57	25	49	25	35	351	34	343
40	Anamba Is.	3°14′	106°15′	13	236	18	267	2	54	6	313	50	15	40	13	29	337	27	328
41	Pulau Laut	4°45′	108°00′	21	84	9	85	7	114	4	86	45	348	36	348	28	293	18	283
42	Natuna	3°48′	108°02′	24	108	21	117	9	140	6	158	43	0	40	355	25	316	27	325
43	Subi Kechil	3°03′	108°51′	49	102	49	109	15	147	15	154	39	350	37	350	24	303	24	303
44	Tanjong Datu	2°05′	109°39′	99	108	91	117	29	158	18	141	42	343	37	335	29	293	15	256
45	Kuching	1°34′	110°21′	174	115	149	131	49	166	46	189	50	341	47	348	35	286	35	293
46	Triso Darat	1°31′	111°00′	194	120	171	143	54	174	52	213	51	343	40	351	36	288	34	313
47	Kuala Paloh	2°27′	111°14′	135	110	110	114	36	160	30	176	47	336	46	338	33	280	37	288
48	Batang Mukah	2°54′	112°05′	63	93	37	93	13	121	9	107	44	323	40	326	35	267	34	268
49	Miri	4°23′	113°59′	16	347	15	341	8	11	9	22	35	311	37	324	31	257	30	271
50	Labuan	5°17′	115°15′	23	329	27	322	11	2	12	8	35	310	40	320	31	257	34	262
51	Kota Kinabalu	5°52′	115°59′	22	324	23	314	10	358	9	353	34	310	35	314	30	257	30	264
52	Balabak I.	8°00′	117°04′	19	318	24	314	8	354	12	351	32	311	30	323	29	258	30	273
53	Ulugan bay	10°04′	118°46′	18	306	21	304	8	345	9	345	30	309	34	317	27	258	27	267
54	Kulion I.	11°48′	119°57′	17	299	24	303	7	335	9	4	28	309	30	318	26	259	30	268
55	Lubang I.	13°49′	120°12′	16	294	20	290	6	330	8	333	27	309	29	310	25	259	26	266
56	Olongapo	14°49′	120°17′	15	291	17	287	5	329	6	324	27	309	27	316	24	258	25	267
57	Santa Cruz	15°46′	119°54′	13	282	12	263	4	322	2	324	25	308	26	313	22	257	22	259
58	San Fernando	16°37′	120°18′	12	268	8	264	3	302	2	283	22	307	24	312	20	256	20	267
59	Yongshujiao	9°33′	112°53′	17	323	18	319	8	0	8	356	32	309	35	311	28	256	29	263
60	Makung	23°33′	119°34′	85	330	87	326	22	29	23	15	26	280	25	278	22	234	21	237
61	Kaohsiung	22°37′	120°16′	20	229	15	236	6	240	6	248	19	276	16	295	17	231	15	249
62	Putai	23°23′	120°09′	55	301	60	312	12	353	14	5	22	274	20	278	20	229	19	237
63	Taichung	24°11′	120°29′	177	331	148	327	51	23	37	16	29	276	18	268	23	231	15	222

Note: g is phase-lag (in deg) referred to 120°E[a], H is amplitude (in cm).

[a]The relations between the Greenwich phase-lags G and the Beijing time phase-lags g are expressed by $G_C = g_C - 8\omega_C$, with C standing for constituents, $\omega_C = 28.984$, 30.000, 15.041 and 13.943 for M_2, S_2, K_1 and O_1, respectively (in degrees per hour).

[b]Harmonic constants calculated by the Admiralty Method.

Table 2
Average absolute values of differences between computed and observed harmonic constants

Method of averaging	M_2		S_2		K_1		O_1	
	H (cm)	g (deg)	H (cm)	g (deg)	H (cm)	g (deg)	H (cm)	g (deg)
Differences averaged for all 63 stations listed in Table 1	6.5	9.9	2.7	17.8	4.6	8.7	3.0	10.6
Differences averaged for 58 stations excluding 5 stations with harmonic constants calculated by the Admiralty Method	6.5	9.4	2.5	14.0	4.5	7.1	2.7	9.9

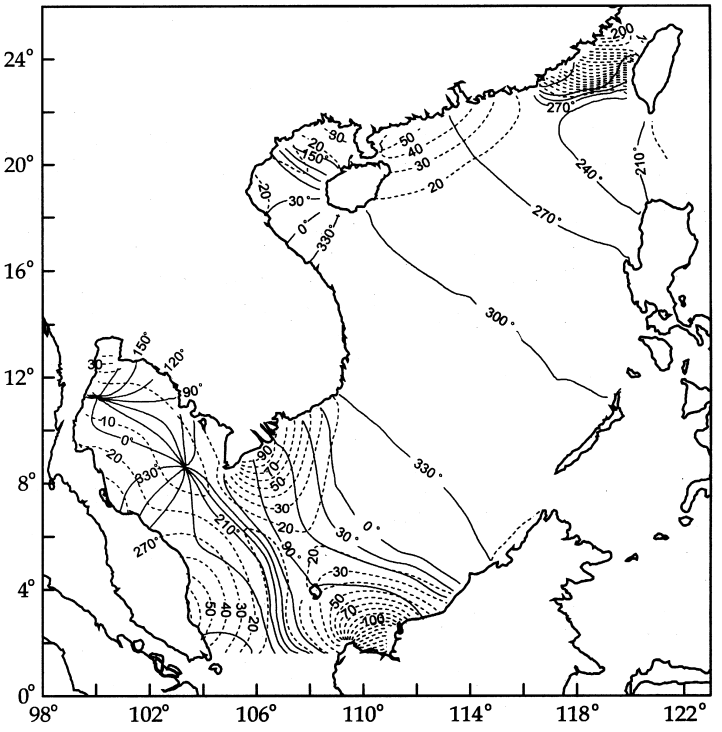

Fig. 3. Model-produced cotidal chart for M_2 constituent. Solid line: phase-lag (in deg), dashed line: amplitude (in cm).

Taiwan Strait. The wave from the South China Sea propagates northward with higher amplitudes on the right side, resulting a northward propagating nature off the southwest coast of Taiwan. The semidiurnal tides in the East China Sea are significantly larger than in the South China Sea, accordingly, the southwestward incident

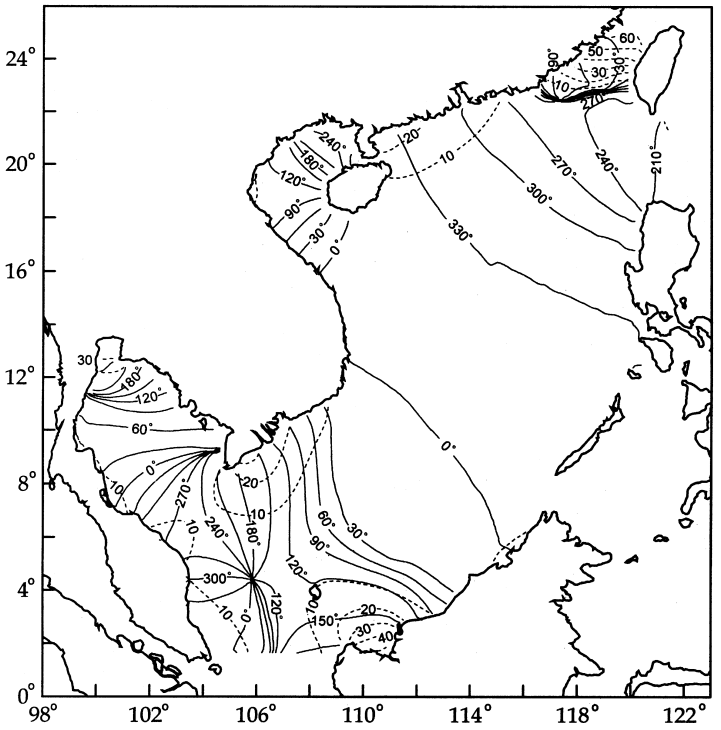

Fig. 4. As in Fig. 3 but for S_2.

wave is also significantly stronger than the northward one. As a result, the nodal band appears near the southern opening of the Taiwan Strait.

In the Gulf of Tonkin, a nodal band can be observed northwest of the Hainan Island. The cotidal lines appear as a degenerate amphidrome with smallest amplitude near Hongai (station No. 15 in Fig. 2). The overall magnitude of M_2 tide in the Gulf of Tonkin is significantly smaller than both K_1 and O_1 tides (Figs. 5 and 6).

Besides the northwest Taiwan Strait, three regions of large tidal ranges can be observed in the South China Sea (Fig. 3). The highest amplitude (exceeding 1.7 m) appears off the southern part of the northwest coast of Kalimantan. The next (exceeding 0.9 m) appears in the vicinity of the estuary of the Mekong River. The third (about 0.7 m) appears northeast of the Leizhou Peninsula (a peninsula to the north of Nainan). By comparing M_2 chart with K_1 or O_1 chart it can be seen that the amplification of semidiurnal tides in the shelf sea east of the Leizhou Peninsula is much greater than diurnal tides. This feature was explained by Cao and Fang (1990) by means of the theory of Clarke and Battisti (1981).

The tidal regime of S_2 is rather similar to that of M_2 (Fig. 4). But an additional amphidromic point can be observed in the northeast South China Sea, where M_2 system appears as a nodal band. This point was first presented in Yu (1984), though the position of the point given by Yu seemed to be too far from the shore. The

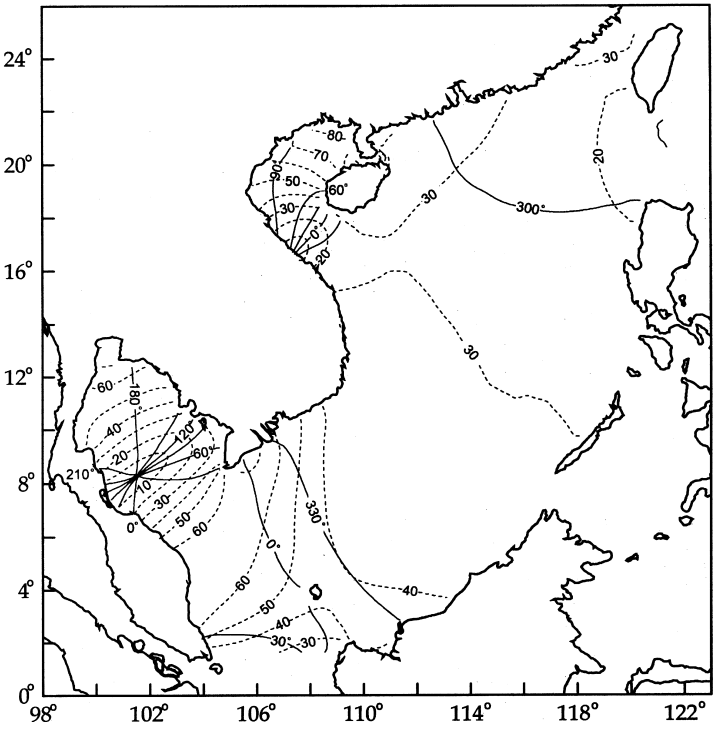

Fig. 5. As in Fig. 3 but for K_1.

existence of this point can be verified by the observed harmonic constants at tidal stations. A one-month observation at Zishen (22°58′N, 116°31′E) shows that the amplitude of S_2 is 2 cm, and the phase-lag is 136°. Combining with the harmonic constants at Shantou and Shanwei listed in Table 1, we may conclude that along the shore the S_2 wave propagates southwestwards and the amphidromic point is close to the shore. Another model-produced S_2 amphidromic point is located west of the Natuna Island. M_2 tide has a corresponding point, but it is located to the south outside the present computational domain (see Fang, 1986, Fig. 6).

The diurnal tides also propagate from northeast to southwest (Figs. 5 and 6). In the Taiwan Strait no northward propagating diurnal wave can be seen from the cotidal charts. The model results show that at the entrance of the Gulf of Tonkin each of O_1 and K_1 tide has a degenerate amphidromic system centered at the middle Vietnam coast. From the observed harmonic constants at station Nos. 17–19 of Table 1, one may see that the O_1 system is definitely degenerate and the K_1 system is marginally degenerate. The K_1 and O_1 constituents respectively form their amphidromic systems in the Gulf of Thailand. Both of them rotate anticlockwise; this is normal in the Northern Hemisphere and quite different from the semidiurnal systems. A possible mechanism is that the ratios of f/σ for diurnal tides are about twice as great as those for semidiurnal tides.

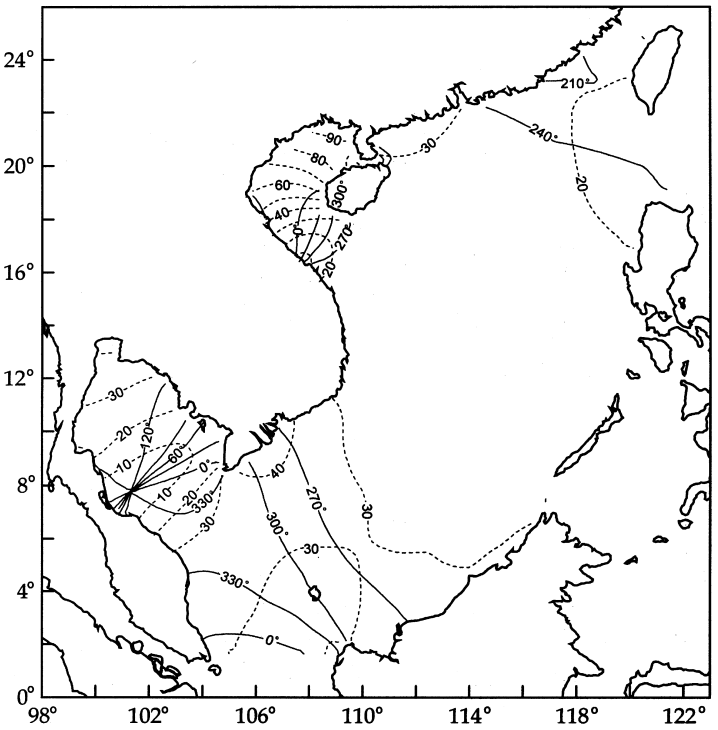

Fig. 6. As in Fig. 3 but for O_1.

Though the K_1 and O_1 tides have smaller magnitudes than M_2 at the Luzon Strait, which is the major opening of the South China Sea, they become dominant constituents in the most parts of the sea. The greatest amplitude of K_1, exceeding 80 cm, is at the closed end of the Gulf of Tonkin; here the amplitude of O_1 is even greater, exceeding 90 cm. The strong diurnal tides can be attributed to the closeness of the free oscillation period of the Gulf to the periods of the diurnal tides, especially to that of O_1. The length of the Gulf of Tonkin is about 500 km and the mean water depth is 50 m. Thus, the period of the lowest mode of free oscillations is approximately 25.1 h, which is very close to the period of O_1.

It is noteworthy that the ratio of amplitudes, H_{O_1}/H_{K_1}, varies from place to place in the South China Sea. We may use the ratios at Yongshujiao (station No. 59 in Table 1 and Fig. 2), Xiamen (No.1), Beihai (No. 13) and Bangkok bar (No.32) to represent the deep basin, Taiwan Strait, Gulf of Tonkin and Gulf of Thailand, respectively. The observed ratio H_{O_1}/H_{K_1} are respectively 0.83, 0.79, 1.09 and 0.69. Thus the response in diurnal band for the Gulf of Tonkin and the Gulf of Thailand possesses quite different characteristics from that of the Taiwan Strait and the main body of the South China Sea.

The maximum velocities of M_2 and O_1 tidal currents are plotted in Figs. 7 and 8. In the deep basin of the South China Sea, tidal currents are very weak, generally below

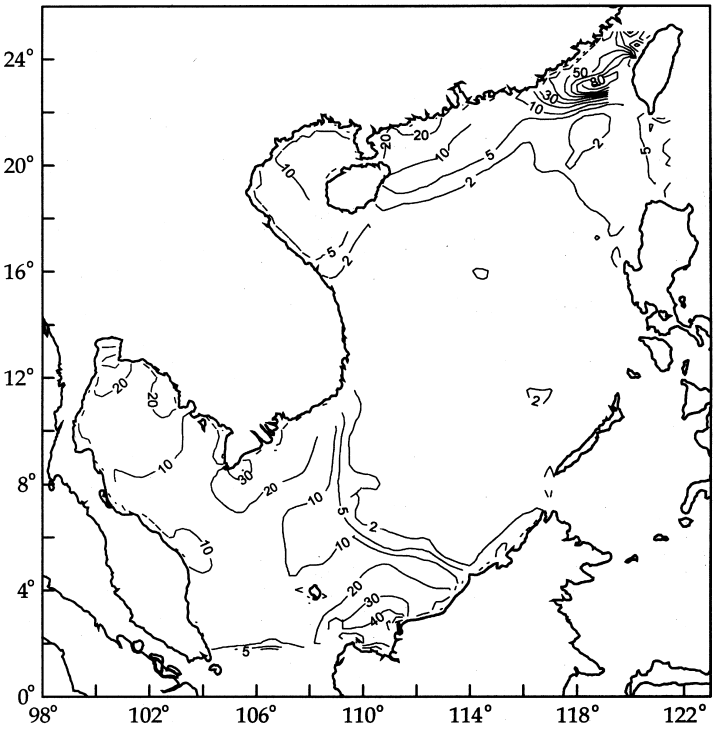

Fig. 7. Maximum velocity of M_2 tidal current (cm/s).

2 cm/s. The strongest M_2 tidal current occurs in the Taiwan Strait, where it may exceed 100 cm/s. The M_2 currents off the southern part of the northwest coast of Kalimantan and off the Mekong River estuary, Southeast Vietnam are also strong. The strongest O_1 tidal current occurs in the Hainan Strait (the Strait between the Hainan Island and the mainland China). Off the west coast of the Hainan Island and at the entrance of the Gulf of Thailand, the diurnal tidal currents are relatively strong.

4.2. Energy balance

Garrett (1975) proposed a tidal energy equation for the linear case, which can be written in the form:

$$F + E = D. \tag{8}$$

Here, F represents the energy flux into the studied area through its openings, E is the rate of work done by the horizontal tidal force, and D stands for the frictional dissipation rate. The energy flux F can be calculated by

$$F = -\rho g \int_B h\langle \zeta u_n \rangle \mathrm{d}l, \tag{9}$$

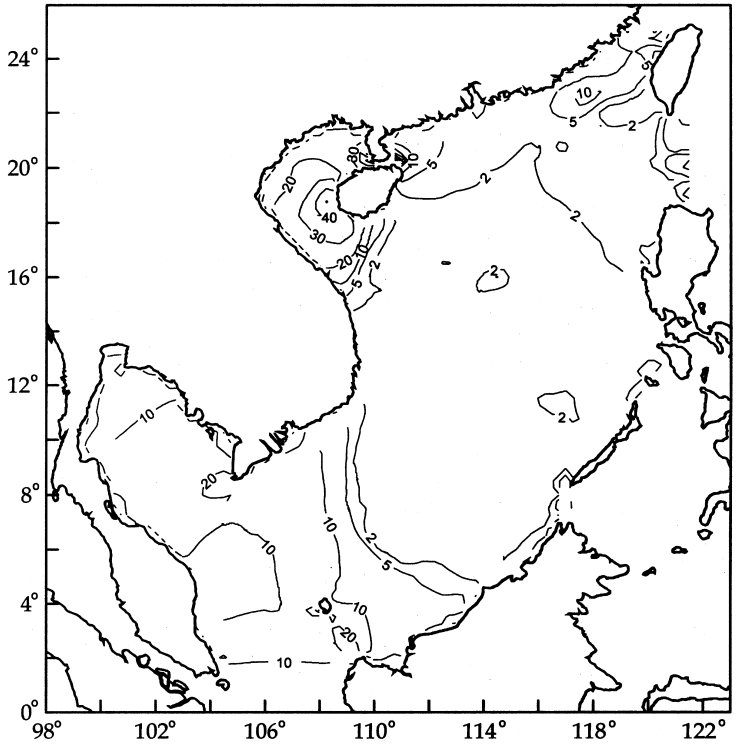

Fig. 8. Maximum velocity of O_1 tidal current (cm/s).

where B represents the openings of the study sea area G, dl is a differential length element on B, u_n is the outward pointing normal component of the current velocity and the angled brackets represent time averaging of the quantity inside. The rate of work of the horizontal force can be calculated by

$$E = \rho g \int\int_G h\langle \mathbf{u} \cdot \nabla \bar{\zeta} \rangle \, dS, \tag{10}$$

where dS is a differential element of the area G. Garrett (1975) gave an alternative form for (10) as follows:

$$E = \rho g \int_B h\langle \bar{\zeta} u_n \rangle \, dl + \rho g \int\int_G \langle \bar{\zeta}(\partial \zeta / \partial t) \rangle \, dS. \tag{11}$$

Eq. (11) was employed by Ye and Robinson (1983) to calculate energy input of the tidal forcing.

In the linear case one can calculate the energy balance of each constituent separately, as done by Ye and Robinsion (1983). Since multiple constituents are simulated simultaneously in the present study, the tidal energy equation needs to be generalized.

Like ζ, u and v themselves, we can apply harmonic analysis using numerical approximation for the nonlinear terms in the Eqs. (1)–(3), where these terms are expanded in Fourier forms:

$$
\begin{aligned}
&-a^{-1}[\partial_\lambda(\zeta u)+\partial_\phi(\zeta v\cos\phi)]=\sum Z_C\cos[\omega_C t+(V_0+u)_C-\gamma_C]\equiv\sum z_C,\\
&-a^{-1}u\partial_\lambda u-R^{-1}v\partial_\phi u+R^{-1}uv\tan\phi=\sum X_C\cos[\omega_C t+(V_0+u)_C-\alpha_C]\equiv\sum x_C,\\
&-a^{-1}u\partial_\lambda v-R^{-1}v\partial_\phi v-R^{-1}u^2\tan\phi=\sum Y_C\cos[\omega_C t+(V_0+u)_C-\beta_C]\equiv\sum y_C,\\
&rH^{-1}(u^2+v^2)^{1/2}u=\sum P_C\cos[\omega_C t+(V_0+u)_C-\chi_C]\equiv\sum p_C,\\
&rH^{-1}(u^2+v^2)^{1/2}v=\sum Q_C\cos[\omega_C t+(V_0+u)_C-\psi_C]\equiv\sum q_C.
\end{aligned}
\tag{12}
$$

The number of harmonic terms contained in Eq. (12) is larger than that in Eq. (4) or Eq. (5). However, by means of some standard tidal harmonic analysis method, such as that proposed by Wang and Fang (1981), the four principal constituents can be well isolated. For a specific constituent C, Eqs. (1), (2) and (3) become correspondingly

$$\partial_t\zeta_C=-a^{-1}[\partial_\lambda(hu_C)+\partial_\phi(hv_C\cos\phi_C)]+z_C, \tag{13}$$

$$\partial_t u_C=x_C+fv_C-p_C-ga^{-1}\partial_\lambda(\zeta_C-\bar{\zeta}_C)+A\,\Delta u_C, \tag{14}$$

$$\partial_t v_C=y_C-fu_C-q_C-gR^{-1}\partial_\phi(\zeta_C-\bar{\zeta}_C)+A\,\Delta v_C, \tag{15}$$

Multiplying Eqs. (13), (14) and (15) by $\rho g\zeta_C$, ρhu_C and ρhv_C respectively and adding them, then taking average for a period, and finally integrating over the area G, these yield

$$F+E+N=D_b+D_l, \tag{16}$$

where the subscript C has been dropped, F and E are expressed by Eqs. (9) and (10), and

$$N=\rho\iint_G(h\langle ux\rangle+h\langle vy\rangle+g\langle\zeta z\rangle)\,\mathrm{d}S, \tag{17}$$

$$D_b=\rho\iint_G(h\langle up\rangle+h\langle vq\rangle)\,\mathrm{d}S, \tag{18}$$

$$D_l=\rho\iint_G hA\langle|\nabla u|^2+|\nabla v|^2\rangle\,\mathrm{d}S. \tag{19}$$

Comparing with the linear case, Eq. (16) has an extra forcing term, which results from the nonlinear interaction. Here, D_b and D_l represent the dissipation rates caused by the bottom and lateral friction respectively. In the derivation of Eq. (19) we have neglected the lateral friction at sidewalls due to the assumed slip lateral boundary condition.

To make a simultaneous analysis of the energy budget in the entire South China Sea and its individual subareas, we divide the studied area into four parts, namely, the

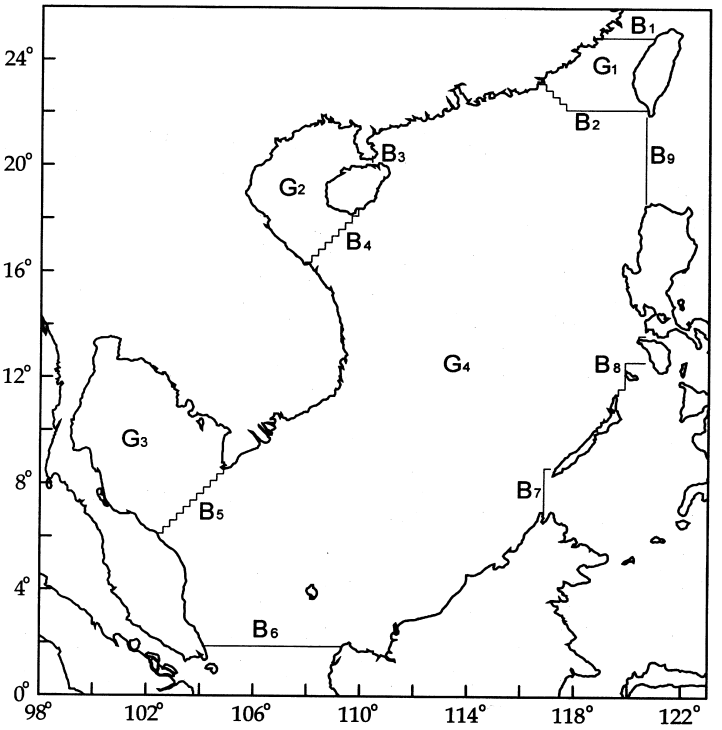

Fig. 9. Subareas of the South China Sea. The tidal energy budget is studied for each subarea and the entire South China Sea.

Taiwan Strait, the Gulf of Tonkin, the Gulf of Thailand and the remaining area. These areas are denoted by G_1, G_2, G_3 and G_4 respectively, as shown in Fig. 9. The boundaries of these subareas are marked with B_1–B_9.

The calculated energy fluxes F through each boundary are listed in Table 3. From the table, we observe that the tides in the South China Sea are essentially maintained by the energy fluxes from the Pacific Ocean through the Luzon Strait (B_9 in Fig. 9). Although the energy fluxes of the semidiurnal tides through the northern boundary of the Taiwan Strait (B_1) are substantial, they are mostly dissipated within the Strait. The energy fluxes through the southern boundary of the Strait (B_2) listed in Table 3 are toward northeast, implying that over there the northeastward semidiurnal waves are stronger than the southwestward ones. For the diurnal tidal waves, the energy fluxes through B_2 section are southwestward, but they are very small compared to the fluxes through the Luzon Strait.

The energy flux across a section of unit width is called flux density. The vectors of the energy flux density for M_2 and O_1 tides are plotted in Figs. 10 and 11. These figures clearly show that the strongest energy fluxes appear in the Luzon Strait for both diurnal and semidiurnal tidal waves. In the Taiwan Strait, the diurnal tidal

Table 3
Energy fluxes through the boundaries of the subareas of the South China Sea (GW)

No. of boundary	Direction of positive flux	M_2	S_2	K_1	O_1
1	S	6.23	1.33	0.68	0.39
2	N&E	8.39	0.36	−0.20	−0.13
3	W	−0.11	−0.02	0.07	−0.11
4	N&W	1.05	0.12	4.48	5.56
5	N&W	1.06	0.23	4.96	1.71
6	N	−2.22	−0.28	−8.26	−6.01
7	N&W	−0.44	−0.00	−3.52	−3.67
8	N&W	−0.99	−0.06	−2.07	−2.96
9	W	29.45	3.17	27.76	21.26

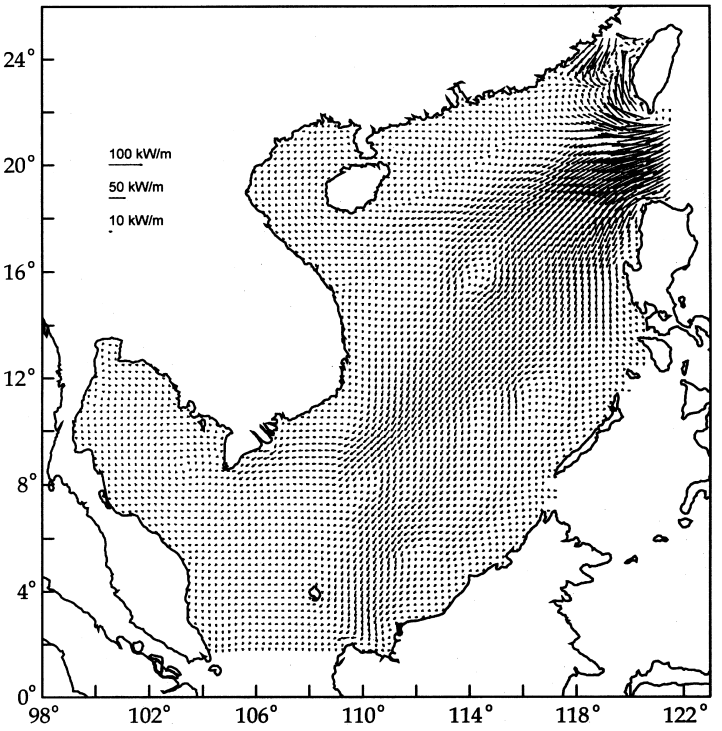

Fig. 10. Tidal energy flux density vectors of M_2 constituent.

energy flux is weak, but the semidiurnal tidal flux is rather strong. The latter is featured by the southward energy flux in the western Strait and the northward energy flux in the eastern Strait. The major branch of energy flux is southwestward passing through the deep basin. The branch toward the Gulf of Tonkin is weak for the

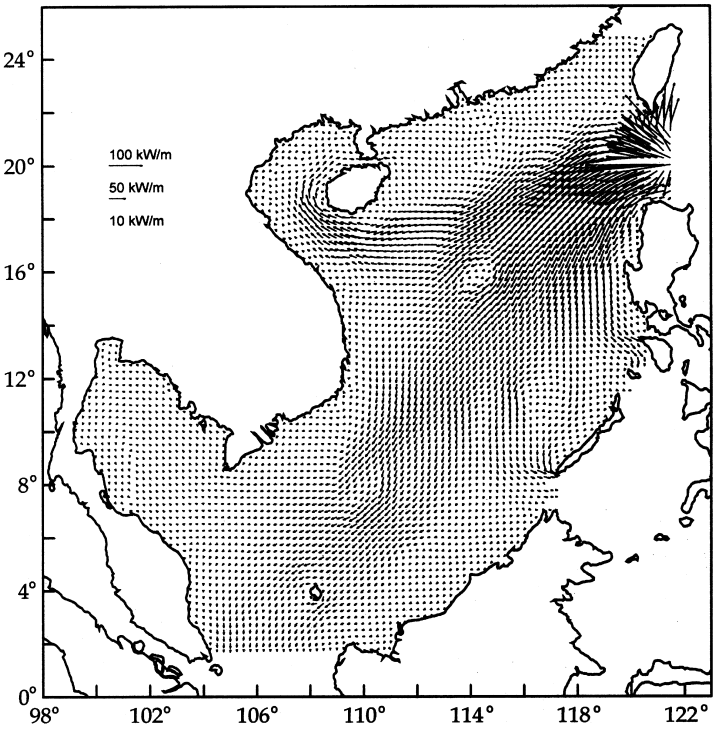

Fig. 11. Tidal energy flux density vectors of O_1 constituent.

semidiurnal tide and rather strong for the diurnal tide. The branches toward the Gulf of Thailand are weak for both semidiurnal and diurnal tides.

The energy budgets for the entire South China Sea and its subareas are shown in Table 4. The energy inputs from the tide-generating force are negative for the semidiurnal tides. This characteristic agrees with the conclusion of Ye and Robinson (1983). But the value of the M_2 tide calculated by the present model is -5.92 GW and is about half of that computed by Ye and Robinson (1983). We have also used Eq. (11) to calculate the values of E, the results were the same as those obtained from Eq. (10). The discrepancy between the results of the present model and Ye and Robinson's model for semidiurnal tides may originate from the difference in the model-produced phase-lags. Table 4 shows that the energy inputs from the diurnal tide-generating force are positive, contrary to the results of Ye and Robinson (1983). This is due to their incorrect expression for the phase of the diurnal equilibrium tide.

We have examined the energy inputs from the S_2 atmospheric tide. The results are 0.007, -0.003, 0.002 GW for the Taiwan Strait, Gulf of Tonkin, Gulf of Thailand respectively and -0.001 GW for the entire South China Sea. The values listed in Table 4 have already included the inputs from the S_2 atmospheric tide.

Table 4
Tidal energy budget in the South China Sea and its subareas(GW)

	M_2					S_2					K_1					O_1				
Area	F	E	N	D_b	D_l	F	E	N	D_b	D_l	F	E	N	D_b	D_l	F	E	N	D_b	D_l
G_1	14.62	0.07	0.00	13.56	0.96	1.69	−0.01	0.00	1.56	0.08	0.48	−0.03	−0.02	0.38	0.03	0.26	−0.01	−0.02	0.22	0.02
G_2	0.94	−0.11	−0.14	0.62	0.04	0.10	−0.01	0.00	0.09	0.01	4.55	0.18	0.05	4.47	0.22	5.45	0.07	0.05	5.22	0.26
G_3	1.06	−0.10	0.00	0.87	0.03	0.23	−0.02	0.00	0.20	0.01	4.96	0.08	−0.05	4.95	0.08	1.71	0.10	−0.04	1.69	0.02
G_4	15.41	−5.92	0.04	9.04	0.69	2.14	−1.18	−0.01	1.02	0.06	4.60	5.09	−0.02	5.65	0.77	1.59	3.59	−0.02	3.92	0.66
G	32.03	−6.06	−0.10	24.09	1.72	4.16	−1.22	−0.01	2.87	0.16	14.59	5.32	−0.04	15.45	1.10	9.01	3.75	−0.03	11.05	0.96

	$F+E+N$	D_b+D_l	$F+E+N$	D_b+D_l	$F+E+N$	D_b+D_l	$F+E+N$	D_b+D_l
G_1	14.69	14.52	1.68	1.64	0.43	0.41	0.23	0.24
G_2	0.69	0.66	0.09	0.10	4.75	4.69	5.52	5.48
G_3	0.92	0.90	0.21	0.21	5.06	5.03	1.78	1.71
G_4	9.53	9.73	0.95	1.08	6.34	6.42	4.43	4.58
G	25.87	25.81	2.93	3.03	16.58	16.55	11.96	12.01

G_1 – Taiwan Strait, G_2 – Gulf of Tonkin, G_3 – Gulf of Thailand, G_4 – the remaining area, G – South China Sea.
F – Rate of energy inflow across boundary, E-rate of work done by tide-generating force, N-rate of energy input through nonlinear effects.
D_b – Dissipation due to bottom friction, D_l – dissipation due to lateral friction.

The energy transfer between constituents can be seen from the values of N in Table 4, and is generally insignificant. However, it is worth noticing that the nonlinear energy input of M_2 in the Gulf of Tonkin is of certain importance.

From Table 4 we observe that the total energy income, $F + E + N$, is basically in balance with the total consumption, $D_b + D_l$. The difference between them are small and may be attributed to the errors caused by numerical discretization.

5. Concluding remarks

The cotidal charts in the South China Sea have been drawn by a number of investigators. The discrepancies among them, especially for semidiurnal tides, are significant. This is due to the sparsity of tidal stations, the complexity of the semidiurnal tidal systems and the inadequacy of previous numerical studies. The comparison of the results produced from the present model with the observational data shows that the cotidal charts of the present model are basically reliable for the principal constituents. The locations for some amphidromic points, such as those of M_2 and S_2 in the Gulf of Thailand and S_2 in the northeastern South China Sea, are clarified through the present study. Though the improvement of the present results over previous studies is obvious, greater efforts are still needed to accurately map the tides of the South China Sea. First of all, the coastal and offshore measurements with tidal gauges are the preliminary task. In particular, the observed harmonic constants along the northeast and northwest shores of the Gulf of Thailand and in the area west of Natuna are very useful in verifying the model results. Accurate harmonic constants at the Luzon strait are also very important in providing the proper open boundary conditions. With the accumulation of the altimetry data collected by satellites such as Topex/Poseidon, the numerical models can be further improved by assimilating the altimetry data.

The study on the tidal energy budget shows that the tidal motion in the South China Sea, Gulf of Tonkin and Gulf of Thailand is mainly maintained by the energy flux from the Pacific Ocean through the Luzon Strait except for the Taiwan Strait, where the tidal motion is maintained by the energy fluxes from both the East China Sea and South China Sea. The calculated energy inputs from the tide-generating force are quite different from the results of Ye and Robinson (1983). This indicates that great uncertainty in this regard still remains and further investigation is needed.

Acknowledgements

The present work was supported partially by the National Special Key Project of China No. 85-927-05-02. The authors are indebted to Messrs. Yue Fang, Zexun Wei and Bing Zhang for preparing the figures and to Ms. Xinyi Wang for typing the text. Thanks are extended to the anonymous reviewer for valuable suggestions.

Appendix

A.1. Outline of the numerical scheme used in the present study

The numerical scheme used in the present study is an extended form of the Alternating Direction Implicit (ADI) scheme 2 proposed by Kwok et al. (1995). The grid is the staggered Arakawa -C type. The values of $\zeta_{i,j}$, $u_{i,j}$ and $v_{i,j}$ are computed at the points $(\lambda_0 + i\Delta\lambda, \phi_0 + j\Delta\phi)$, $(\lambda_0 + (i + 1/2)\Delta\lambda, \phi_0 + j\Delta\phi)$ and $(\lambda_0 + i\Delta\lambda, \phi_0 + (j + 1/2)\Delta\phi)$ respectively, where (λ_0, ϕ_0)corresponds to the position of the point $\zeta_{0,0}$. First we introduce the following notation:

$$\alpha \equiv \cos\phi,\ \beta \equiv \sin\phi;\ \Delta x_j \equiv a_j\Delta\lambda \equiv R\alpha_j\Delta\lambda,\ \Delta y \equiv R\Delta\phi;$$

$$D_{+x}u_{i,j} \equiv (u_{i+1,j} - u_{i,j})/\Delta x_j, \quad D_{-x}u_{i,j} \equiv (u_{i,j} - u_{i-1,j})/\Delta x_j,$$

$$D_{ox}u_{i,j} \equiv (u_{i+1,j} - u_{i-1,j})/2\Delta x_j;$$

$$D_{+x}v_{i,j} \equiv (v_{i+1,j} - v_{i,j})/\Delta x_{j+1/2}, \quad D_{-x}v_{i,j} \equiv (v_{i,j} - v_{i-1,j})/\Delta x_{j+1/2},$$

$$D_{ox}v_{i,j} \equiv (v_{i+1,j} - v_{i-1,j})/2\Delta x_{j+1/2};$$

$$u_{i-1/2,j+1/2} \equiv (u_{i,j} + u_{i-1,j} + u_{i-1,j+1} + u_{i,j+1})/4,$$

$$v_{i+1/2,j-1/2} \equiv (v_{i,j} + v_{i+1,j} + v_{i+1,j-1} + v_{i,j-1})/4;$$

$$H_{i+1/2,j} \equiv (h_{i,j} + h_{i+1,j} + \zeta_{i,j} + \zeta_{i+1,j})/2,$$

$$H_{i,j+1/2} \equiv (h_{i,j} + h_{i,j+1} + \zeta_{i,j} + \zeta_{i,j+1})/2;$$

$$C_{xi,j} \equiv r(u_{i,j}^2 + v_{i+1/2,j-1/2}^2)^{1/2}/H_{i+1/2,j},$$

$$C_{yi,j} \equiv r(u_{i-1/2,j+1/2}^2 + v_{i,j}^2)^{1/2}/H_{i,j+1/2};$$

$$\Delta u_{i,j} \equiv (u_{i+1,j} - 2u_{i,j} + u_{i-1,j})/\Delta x_j^2 + [(u_{i,j+1} - u_{i,j})\alpha_{j+1/2} - (u_{i,j} - u_{i,j-1})\alpha_{j-1/2}]/(\Delta y^2\,\alpha_j),$$

$$\Delta v_{i,j} \equiv (v_{i+1,j} - 2v_{i,j} + v_{i-1,j})/\Delta x_{j+1/2}^2 + [(v_{i,j+1} - v_{i,j})\alpha_{j+1} - (v_{i,j} - v_{i,j-1})\alpha_j]/(\Delta y^2\,\alpha_{j+1/2});$$

$$L_{xi,j} \equiv -u_{i,j}D_{ox}u_{i,j} - v_{i+1/2,j-1/2}[D_{oy}u_{i,j} - (2\Omega + u_{i,j}/a_j)\beta_j] + gD_{+x}\overline{\zeta}_{i,j},$$

$$L_{yi,j} \equiv -u_{i-1/2,j+1/2}[D_{ox}v_{i,j} + (2\Omega + u_{i-1/2,j+1/2}/a_{j+1/2})\beta_{j+1/2}] - v_{i,j}D_{oy}v_{i,j} + gD_{+y}\overline{\zeta}_{i,j},$$

then the governing Eqs. (1)–(3) can be approximated by the following finite-difference scheme to second order accuracy:

$$(I + \Delta t\,P + \Delta t\,Q)w^{n+1} = F, \tag{A.1}$$

where I is the identity matrix and

$$P=\begin{pmatrix} C^n_{xi,j} & 0 & gD_{+x} \\ 0 & C^n_{yi,j} & 0 \\ D_{-x}(H^n_{i+1/2,j}\cdot) & 0 & 0 \end{pmatrix}, \quad Q=\begin{pmatrix} 0 & 0 & 0 \\ 0 & 0 & gD_{+y} \\ 0 & \alpha_j^{-1}D_{-y}(H^n_{i,j+1/2}\alpha_{j+1/2}\cdot) & 0 \end{pmatrix},$$

$$w^{n+1}=\begin{pmatrix} u^{n+1}_{i,j} \\ v^{n+1}_{i,j} \\ \zeta^{n+1}_{i,j} \end{pmatrix},$$

$$F=\begin{pmatrix} u^{n-1}_{i,j}+\Delta t(2L^n_{xi,j}+2A\,\Delta u^{n-1}_{i,j}-C^n_{xi,j}u^{n-1}_{i,j}-gD_{+x}\zeta^{n-1}_{i,j}) \\ v^{n-1}_{i,j}+\Delta t(2L^n_{yi,j}+2A\,\Delta v^{n-1}_{i,j}-C^n_{yi,j}v^{n-1}_{i,j}-gD_{+y}\zeta^{n-1}_{i,j}) \\ \zeta^{n-1}_{i,j}-\Delta t[(H^n_{i+1/2,j}u^{n-1}_{i,j}-H^n_{i-1/2,j}u^{n-1}_{i-1,j})/\Delta x_j \\ \quad +(H^n_{i,j+1/2}v^{n-1}_{i,j}\alpha_{j+1/2}-H^n_{i,j-1/2}v^{n-1}_{i,j-1}\alpha_{j-1/2})/(\Delta y\alpha_j)] \end{pmatrix}.$$

To facilitate ADI factorization, Eq. (A1) is modified as follows:

$$(I+\Delta t\,P+\Delta t\,Q+\Delta t^2\,PQ)w^{n+1}=\Delta t^2\,PQw^{n-1}+F. \tag{A.2}$$

Note that second-order temporal accuracy is maintained. The solution of Eq. (A.2) can be split into two substeps:

$$(I+\Delta t\,P)\tilde{w}=-\Delta t\,Qw^{n-1}+F, \tag{A.3}$$

$$(I+\Delta t\,Q)w^{n+1}=\tilde{w}+\Delta t\,Qw^{n-1}. \tag{A.4}$$

Each of the above equations can be solved effectively through the inversion of a tridiagonal matrix. The boundary condition for Eq. (A.3) can be derived from Eq. (A.4), that is,

$$\tilde{w}=w^{n+1}+\Delta t\,Q(w^{n+1}-w^{n-1}). \tag{A.5}$$

In the South China Sea tidal model, we have only ζ-points on the open boundaries, the value of $\tilde{\zeta}$ can be calculated from

$$\begin{aligned}\tilde{\zeta}_{i,j}&=\zeta^{n+1}_{i,j}+\Delta t\,\Delta y^{-1}\,\alpha_j^{-1}[H^n_{i,j+1/2}\alpha_{j+1/2}(v^{n+1}_{i,j}-v^{n-1}_{i,j}) \\ &\quad -H^n_{i,j-1/2}\alpha_{j-1/2}(v^{n+1}_{i,j-1}-v^{n-1}_{i,j-1})] \\ &\approx\zeta^{n+1}_{i,j}+\Delta t\,\Delta y^{-1}\,\alpha_j^{-1}[H^n_{i,j+1/2}\alpha_{j+1/2}(\tilde{v}_{i,j}-v^{n-1}_{i,j}) \\ &\quad -H^n_{i,j-1/2}\alpha_{j-1/2}(\tilde{v}_{i,j-1}-v^{n-1}_{i,j-1})],\end{aligned} \tag{A.6}$$

where the value of $\tilde{v}$ can be calculated by solving the v component of Eq. (A.3) independently.

The time step is limited by the stability requirement of computations of the advection, Coriolis and lateral friction terms. The full analysis of the stability property of the above scheme is intractable. A conventional approach for choosing Δt is taking the minimum of the time step restrictions associated with the individual terms in the governing equations, that is,

$$\Delta t < \min\left(\frac{1}{\dfrac{|u|}{\Delta x}+\dfrac{|v|}{\Delta y}}, \frac{1}{2\Omega\sin\phi}, \frac{1}{2A\left(\dfrac{1}{\Delta x^2}+\dfrac{1}{\Delta y^2}\right)}\right). \tag{A.7}$$

Furthermore, the leap-frog differencing may introduce a tendency for decoupling between solutions at the even and odd time steps. To circumvent this difficulty, a smoothing procedure is generally required. In the present calculations, only the values of u and v are smoothed at each time step according to,

$$u_s^n = (1-2\varepsilon)u^n + \varepsilon(u^{n+1} + u^{n-1}), \tag{A.8}$$

where u_s is the smoothed value and ε is a small quantity. In the present South China Sea tidal model, we take $\varepsilon = 0.0025$.

References

Bogdanov, C.T., 1963. Propagation of tidal waves and characteristic tidal oscillation of level in the Australo-Asiatic Seas. Trudy Institute Oceanology 66, 59–65 (in Russian, English abstract).

Cao, D., Fang, G., 1990. A numerical model for tides and tidal currents in northern South China Sea. Tropic Oceanology 9, 63–70 (In Chinese, English abstract).

Cao, D., Fang, G., Huang, Q., Yu, K., Wang, X., 1997. Tidal regime in the Nansha Sea area and its adjacent southwest waters. Oceanologia et Limnologia Sinica 28, 198–208 (In Chinese, English abstract).

Chapman, S., Lindzen, R.S., 1970. Atmospheric Tides. Reidel, Dordrecht.

Clarke, A.J., Battisti, D.S., 1981. The effect of continental shelves on tides. Deep-Sea Research 28, 665–682.

Fang, G., 1980. Nonlinear effects of tidal friction (I), Oceanologia et Limnologia Sinica 11, 98–108 (In Chinese, English version appeared in Acta Oceanologica Sinica 6 (Suppl. I), 105–122, 1987).

Fang, G., 1981. Nonlinear effects of tidal friction (II), Oceanologia et Limnologia Sinica 12, 195–209 (In Chinese, English version appeared in Acta Oceanologica Sinica 6 (Suppl. I), 105–122, 1987).

Fang, G., 1986. Tide and tidal current charts for the marginal seas adjacent to China. Chinese Journal of Oceanology and Limnology 4, 1–16.

Fang, G., Yang, J., Thao, Y. 1984. A two-dimensional numerical model for tidal motion in the Taiwan Strait. Marine Geophysical Research 7, 267–276.

Garrett, C., 1975. Tides in gulfs. Deep-Sea Research 22, 23–35.

Kwok, Y.-K., Wu, L., Pan, H., 1995. Second order accurate scheme for numerical simulation of shallow water flows. Proceedings of the First Asian Computational Fluid Dynamics Conference, pp. 16–19.

Nguyen, N.T., 1969. Some peculiarities of the formation of tidal phenomena in the South China Sea. Okeanologiia 9, 235–249 (in Russian, English abstract).

Pugh, D.T., 1987. Tides, Surges and Mean Sea-Level. Wiley, Chichester, 471pp.

Sager, G., 1975. Die gezeiten des Sudchinesischen Meeres. Beitrage zur Meereskunde 36, 95–110.

Sergeev, J.N., 1964. The application of the method of marginal values for the calculation of charts of tidal harmonic constants in the South China Sea. Okeanologiia 4, 595–602 (in Russian, English abstract).

Wahr, J., 1981. Body tides on an elliptical, rotating elastic and oceanless earth. Geophysical Journal of the Royal Astronomical Society 64, 677–703.

Wang, J., Fang, G., 1981. An analysis of incomplete hourly tidal records. Acta Oceanologica Sinica 3, 193–210 (in Chinese, English abstract).

Ye, A.L., Robinson, I.S., 1983. Tidal dynamics in the South China Sea. Geophysical Journal of the Royal Astronomical Society 72, 691–707.

Yu, M., 1984. A preliminary study of tidal characteristics in the South China Sea. Acta Oceanologica Sinica 6, 293–300 (in Chinese).